Mineral chemistry of leucitites from Visoke Volcano (Virunga Range, Rwanda): petrogenetic implications

G. MARCELOT

Laboratoire de Pétrologie, Université de Bretagne Occidentale 29287 Brest Cedex, France

AND

J. PH. RANÇON

Bureau de Recherches Géologiques et Minières, Département Géologie, BP 6009, 45060 Orléans Cedex, France

Abstract

The Visoke complex is one of the main Quaternary volcanic centres of the Virunga Range, located north of lake Kivu. Mineralogical (microprobe) data are given for two representative leucitite lavas; one sample contains a complex coarse-grained xenolith (phlogopite, diopside, leucite, titanomagnetite, perovskite and apatite) and megacrysts of pyroxene, phlogopite and olivine scattered in fine-grained leucite-rich host lava. Compared with the typical leucite-dominated, low-pressure phenocryst assemblage of the two samples studied, the chemical trends of ferromagnesian crystals suggest an earlier igneous event (high-pressure phenomenon) strongly related to the leucite-bearing magma suite.

KEYWORDS: mineral chemistry, leucitites, Visoke Volcano, Rwanda.

Introduction

LEUCITE-BEARING rocks, notably leucitite and leucite basanite, form a rare group of alkaline mafic or ultramafic rocks. Besides leucite, these lavas may contain variable amounts of clinopyroxene, amphibole, mica, olivine, feldspathoid, magnetite, apatite and secondary minerals. Because of their unusual mineralogy and chemistry, diverse hypotheses have been proposed to account for their origin. A discussion of these theories is given by Gupta and Yagi (1980), probably the most favoured being those involving low degrees of partial melting of K-enriched mantle rocks. However, further studies appear necessary to establish the relationship between mineralogical and chemical characteristics of the source material and the various trends of such potassic magma suites.

The Virunga range, in East Africa, is one of the major highly potassic petrographic provinces. Although each eruptive centre displays its own chemical individuality, the volcanic association includes a large volume of leucite-bearing rocks (Thonnard et al., 1965; Denaeyer, 1972; Denaeyer

and Schellinck, 1965; Bell and Powell, 1969; Pouclet, 1976; Guibert, 1978; Pouclet et al., 1983).

The Visoke is one of the eight central volcanoes of the Virunga range (Fig. 1) and has produced leucitite, olivine nephelinite, basanite and hawaiite lavas (Pouclet, 1977; Rançon and Demange, 1983). The purpose of this paper is to describe the mineralogical assemblage of two particularly interesting leucitite samples from the volcano.

Petrographic and chemical notes

According to Denaeyer and Schellinck (1965), the Visoke leucitites exhibit a relatively restricted compositional range. All the lavas have a highly porphyritic character and are rich in modal leucite, usually forming 20–30% of the phenocrysts. The samples discussed in this paper were collected from lava flows on the summit (RW 100) and at the base of the cone (RW 37). These rocks are light grey (RW 37) or brownish grey (RW 100), vesicular and porphyritic, in which large crystals of leucite, dark pyroxene and reddish brown phlogopite (RW 100) are the more obvious mineral
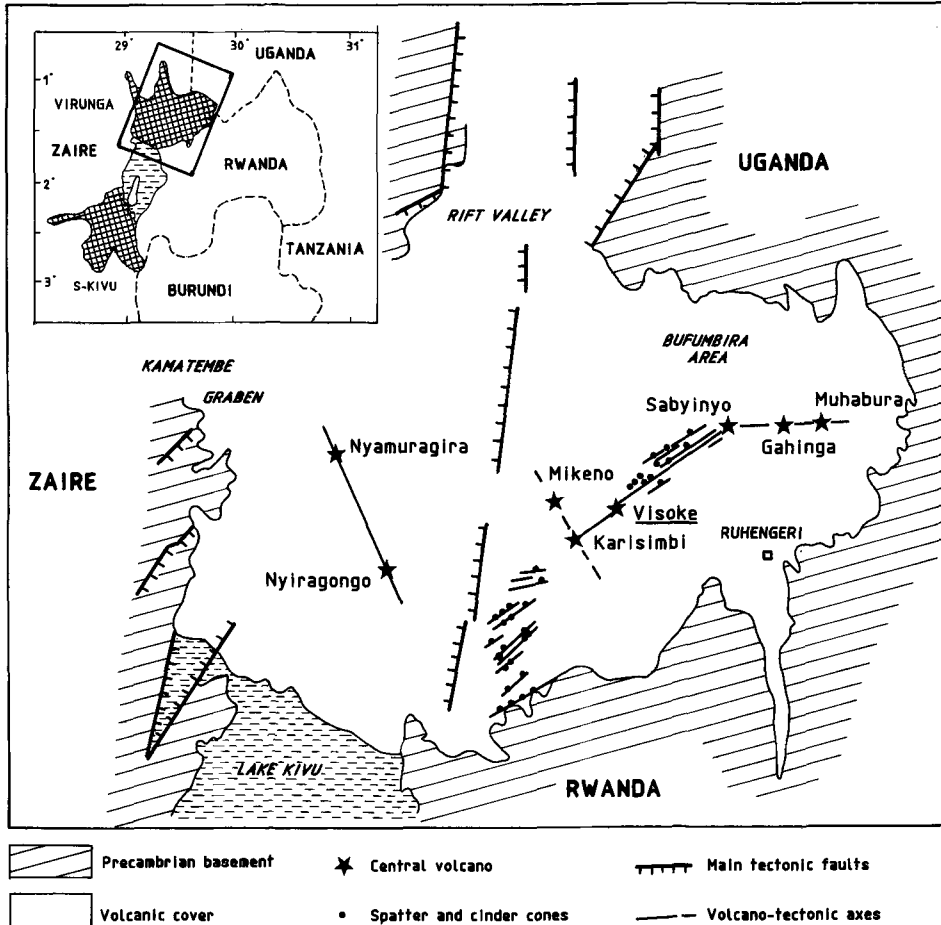
FiG. 1. Location of the Virunga volcanic Range and structural setting of the Visoke volcano.

constituents. The mineralogy of RW 37 is simple; leucite is the most abundant phase and forms euhedral phenocrysts (up to 3 mm in size), associated with phenocrysts of clinopyroxene and Fe–Ti oxides. In the groundmass, nepheline forms large poikilitic patches; other phases are isotropic leucite, pyroxene, Fe–Ti oxides, and apatite.

Sample RW 100 contains a small, rounded, coarser grained xenolith (1–2 cm) composed of megacrysts of leucite, clinopyroxene and phlogopite. Leucite tends to form preferentially as aggregates around ferromagnesian crystals. The matrix of the xenolith consists of fine-grained leucite, pyroxene, ores and apatite. Perovskite and titanomagnetite in variable but limited sizes (< 0.5 mm) are present in the xenolith as phenocrysts. Both minerals always occur together along with some microphenocrysts of pyroxene and phlogopite in the microcrystalline matrix adjacent to the

phenocryst assemblage. The host rock contains some xenocrysts of clinopyroxene, phlogopite and rare olivine scattered in a fine-grained matrix that varies in texture from intersertal to hyalopilitic. Subhedral to euhedral microphenocrysts of leucite, Fe–Ti oxide and pyroxene are common in the lava. These can be distinguished from the xenocrysts by their crystal outline, the former are euhedral and smaller in size, while the latter are irregular, broken and display concentric zoning. The groundmass consists of the same association with apatite and a dark interstitial glass locally preserved.

A relatively sharp contact exists between the outer zone of the xenolith and the host lava, the two mineral assemblages do not show any reaction rim or cross-cutting relationships. However, separation of crystals from the margin of the xenolith has occurred.

Phlogopite only occurs as anhedral crystals in

association with the coarse-grained inclusions or scattered in the host lava. The cores of megacrysts are always unstable and rimmed, and, in a few cases, partly replaced by fine-grained aggregates of Fe–Ti oxides. Usually, the megacrysts appear to be zoned, the rims of the crystals showing the same intense pleochroism as the microphenocrysts.

TABLE 1   Whole rock compositions. Major elements in wt.% and trace elements in ppm

	RW 100	RW 37
SiO₂	39.9	41.9
Al₂O₃	11.40	13.37
Fe₂O₃	5.30	12.56
FeO	7.55	n.d.
MgO	6.60	4.73
CaO	12.70	10.17
Na₂O	3.50	2.03
K₂O	5.15	7.21
MnO	0.22	0.21
TiO₂	5.80	4.52
P₂O₅	0.98	0.90
L.O.I.	n.d.	2.40
Total	99.10	100.00
Rb	158	252
Cs	9	8
Ba	1600	1750
Sr	1534	1113
Li	11	8
V	478	381
Cr	72	41
Co	30	20
Ni	48	35
Cu	134	98
Zn	105	95

Clinopyroxene is universally present. When appearing as a xenocryst it exhibits a typical concentric zonation. The cores, of diopsidic composition, are variable in size, sometimes constituting a substantial proportion (more than 50%) of the total crystal. Generally, the megacrysts as well as the phenocrysts are fresh, clear and without evident inclusions.

Olivine is scarce but when present it occurs near the contact of the xenolith and shows evidence of resorption. Phenocrysts are mantled by a thick reaction zone characterized by a concentration of iron oxides, pyroxene and yellow–brown mica.

Leucite is the most abundant phase and shows variable crystal development. The large leucite crystals are generally twinned indicating a slow rate of cooling through the leucite inversion temperature of 630 °C (Faust, 1963).

Our new major element analyses (Table 1) show very little variation from those given by Denaeyer and Schellinck (1965). The Visoke leucitites are similar in major and trace element chemistry to other occurrences of ultrapotassic mafic rocks (e.g. Gupta and Yagi, 1980). They are noteworthy for their very high Ti, K, P, Rb, Cs, Ba, and Sr, and low Si contents (Marcelot et al., submitted). The Mg values are moderate and indicate, in accordance with Cr and Ni contents, the fractionated character of these lavas (Frey et al., 1978). The Cu/Zn ratios and Ti/V ratios corroborate their strong alkaline affinity (Shervais, 1982). The leucitites are strongly diopside- and leucite-normative, the high (Na + K)/Al ratios of the whole rock (equal to 1 in sample RW 100) indicating a peralkaline tendency.

The chemical differences between the two samples could reflect the abundance of ferromagnesian megacrysts in the lava RW 100, but more probably illustrate a geochemical differentiation.

Mineral chemistry

Mineral analyses (Tables 2–7) were obtained from polished thin sections of analysed bulk rocks by means of an automated Camebax electron microprobe (Microsonde Ouest, Brest, France) operated at 15 kV and 10–12 nA with a counting time of 6 s. The value 0.1% is considered empirically to be the limit of detection below which the given calculated concentrations are not significant.

Leucite. Their structural formulae show a systematic cation deficiency in the X value (Na + K < 1), whereas the Si/Al ratios are generally lower than 2. Such non-stoichiometric analyses in leucite-bearing lavas have been reported and discussed by numerous authors (Carmichael, 1967; Brown and Carmichael, 1969; Cundari, 1975; Van Kooten, 1980).

The megacryst, microphenocryst and groundmass leucites show significant chemical variation. Megacrysts occurring in the xenolith are chemically distinct from both the megacrysts and groundmass host lava crystals in their lower Fe and Na content.

Nepheline has been identified as phenocrysts and as groundmass constituents in sample RW 37. The K₂O contents are always high (4.9 to 9.1 wt. %). Small amounts of Fe, Ca and Mg are also reported in the analysed crystals.

Olivine. The CaO content is high (> 0.50%), as found in olivine phenocrysts from silica undersaturated lavas (Stormer, 1973), and increases with Mn and Fe contents. Simkin and Smith (1970) showed that olivine from volcanic rocks have

TABLE 2   *Nepheline and leucite compositions*

Sample	RW 100					RW 37				
N° of anal.	1	2	3	4	5	6	7	8	9	10
SiO_2	54.65	54.76	53.58	54.32	54.48	56.23	55.04	55.15	42.91	42.48
TiO_2	0.39	0.20	0.33	0.35	0.02	0.32	0.39	0.32	0.00	0.07
Al_2O_3	23.06	23.54	23.90	23.49	22.42	25.30	24.60	24.35	33.29	31.65
FeO	0.29	0.55	0.64	0.70	1.44	0.34	0.61	0.21	1.00	0.79
MnO	0.00	0.00	0.00	0.00	0.00	0.00	0.00	0.00	0.00	0.02
MgO	0.00	0.00	0.00	0.00	0.00	0.00	0.00	0.00	0.15	0.40
CaO	0.00	0.00	0.01	0.00	0.01	0.00	0.00	0.00	0.44	0.61
Na_2O	0.02	0.02	0.13	0.36	0.19	0.69	0.51	0.66	14.84	14.49
K_2O	20.09	19.54	21.84	19.56	21.12	16.98	19.57	17.69	8.32	8.31
Total	98.50	98.61	100.43	98.78	99.68	99.86	100.72	98.38	100.95	98.82
Si	2.002	1.998	1.954	1.988	2.000	1.989	1.968	1.994	8.267	8.375
Ti	0.011	0.005	0.009	0.010	0.001	0.008	0.010	0.009	0.000	0.011
Al	0.995	1.012	1.027	1.013	0.970	1.055	1.037	1.037	7.558	7.355
Fe	0.009	0.017	0.019	0.021	0.044	0.010	0.018	0.006	0.162	0.130
Mn	0.000	0.000	0.000	0.000	0.000	0.000	0.000	0.000	0.000	0.004
Mg	0.000	0.000	0.000	0.000	0.000	0.000	0.000	0.000	0.044	0.117
Ca	0.000	0.000	0.001	0.000	0.001	0.000	0.000	0.000	0.091	0.129
Na	0.002	0.002	0.009	0.011	0.014	0.047	0.035	0.046	5.543	5.540
K	0.939	0.909	1.016	0.913	0.990	0.766	0.893	0.816	2.045	2.089

1 : Core of leucite megacryst included in xenolith
2 : Rim of the same leucite megacryst
3 : Core of leucite microphenocryst (xenolith)
4 : Groundmass leucite (xenolith)
5 : Groundmass leucite (host lava)
6 : Core of leucite megacryst
7 : Rim of the same leucite megacryst
8 : Core of leucite megacryst
9 : Core of nepheline phenocryst
10 : Groundmass nepheline

TABLE 3   *Olivine compositions*

Sample	RW 100			
N° of anal.	1	2	3	4
SiO_2	39.63	39.12	39.11	38.56
FeO	16.22	17.00	19.12	18.33
MnO	0.16	0.17	0.33	0.46
MgO	44.32	44.37	41.74	41.85
CaO	0.55	0.54	0.90	1.02
Total	100.88	101.20	101.20	100.22
Si	0.994	0.983	0.992	0.964
Fe	0.339	0.355	0.405	0.391
Mn	0.004	0.004	0.007	0.010
Mg	1.649	1.653	1.577	1.592
Ca	0.015	0.015	0.024	0.028
Fo %	82.7	82.2	79.3	79.9

1 : Core of phenocryst
2 : Rim of the same phenocryst
3 : Core of microphenocryst
4 : Core of microphenocryst

> 0.1% CaO, while those of intrusive rocks and mantle xenoliths have < 0.1% CaO, which suggests that these olivine xenocrysts have crystallized from a mafic lava rather than representing accidental or extraneous inclusions. Furthermore, the strong enrichment in Ca with decreasing Mg/(Mg + Fe) is consistent with a pressure drop during crystallization.

Titanomagnetite occurs as phenocrysts as well as microlites in the groundmass. It coexists with perovskite in the xenolith, and both are located in the fine-grained matrix adjacent to the ferromagnesian megacrysts as late-crystallized phases. In this case, titanomagnetite has lower TiO_2, MgO and Al_2O_3 contents, but contains appreciable amounts of MnO.

The titanomagnetites are noteworthy for their Al/Mg ratios, notably lower than those of the potassic lavas of Karisimbi volcano which also belongs to the Virunga Range (Fig. 1) (Marcelot *et al.*, 1985). The compositions of Fe–Ti oxides
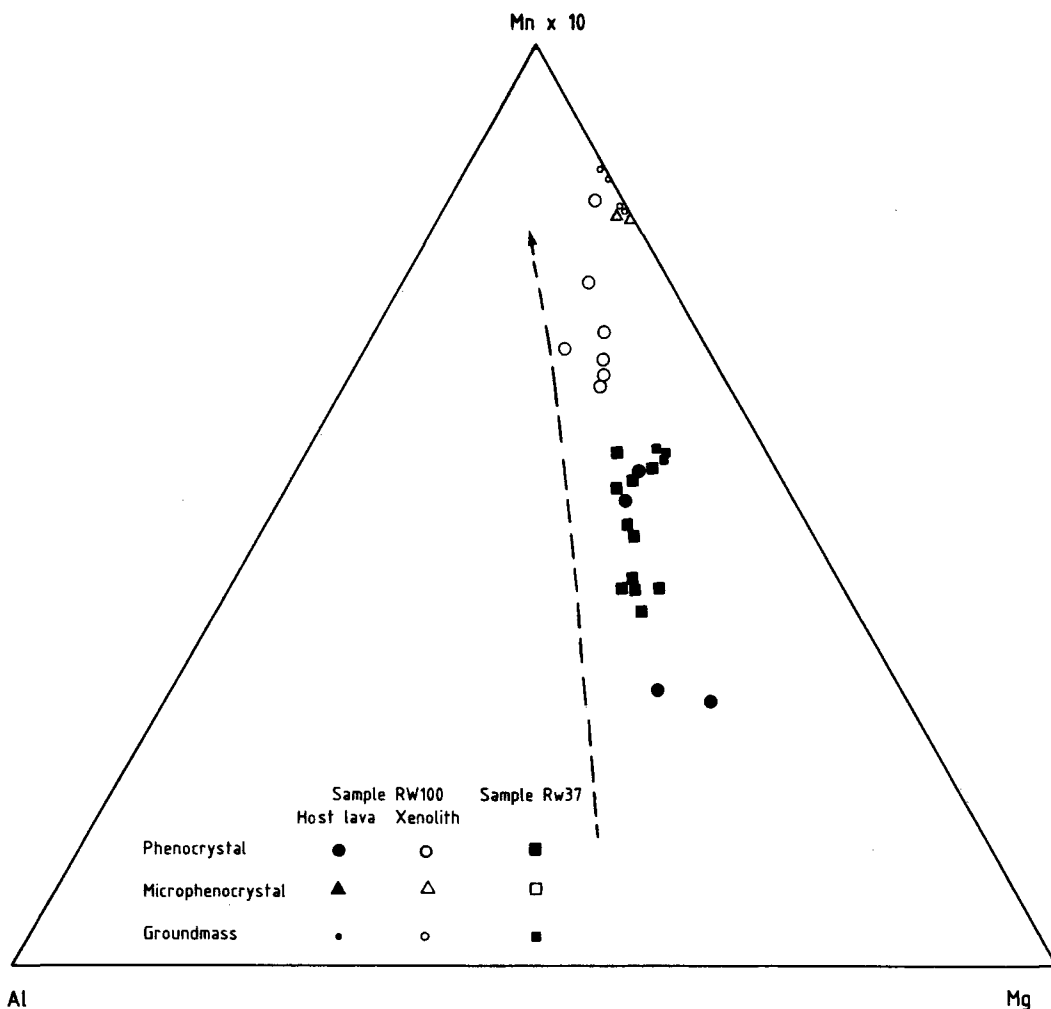
FIG. 2. Chemical trends of iron–titanium oxides. For comparison, Karisimbi oxide trend is shown as dashed line (Marcelot *et al.*, 1985).

plot on well-defined trends of increasing Mn. The phenocrysts of sample RW 100 have the least evolved compositions, whereas xenolith crystals are distinguished by their Al-depleted character (Fig. 2).

Clinopyroxene. The pyroxenes are Ca-rich, transgressing the diopside–hedenbergite join as they become richer in iron as well as in the Ca-Tschermak's and ferri-Tschermak's molecules (Fig. 3).

The pyroxenes occurring as megacrysts and as cores in xenolithic phenocrysts are very similar in composition, and most analyses plot in the diopside field. Diopside crystals are zoned and typically have rims enriched in Al_2O_3, TiO_2 and FeO and

depleted in SiO_2, MgO and Cr_2O_3. Thus, the megacryst rims appear to be close to the phenocrysts and are characterized by $Si + Al < 2.0$ in their structural formulae. Only Cr-diopside shows a slight excess of Al^{3+} over that needed to complete the tetrahedral sites. The cation deficit in the Z-position tends to increase with the decreasing $Mg/(Mg + Fe)$ ratio of the clinopyroxenes. Besides their silica-poor character, pyroxenes have low Al/Ti ratios (< 3) which decrease through the suite diopside–salite. According to their Mg-rich nature, diopside cores have significant Cr_2O_3 contents (0.20–0.30 wt. %).

A plot of Al and Ti against Si in terms of atoms per 6 oxygens (Fig. 4) demonstrates that a good

TABLE 4   Iron - Titanium oxide compositions

| Sample | RW 100 | | | | | RW 37 | | | |
N° of anal.	1	2	3	4	5	6	7	8	9
SiO_2	0.05	0.00	0.00	0.00	0.00	0.15	0.04	0.03	0.20
TiO_2	19.89	20.63	18.19	17.93	21.04	24.24	25.89	25.81	27.11
Al_2O_3	0.28	0.04	1.62	1.43	0.00	3.94	3.16	2.82	1.32
Cr_2O_3	0.18	0.22	0.31	0.55	0.17	0.17	0.15	0.01	0.05
Fe_2O_3*	31.28	30.07	33.31	33.97	29.30	20.25	17.64	18.99	15.82
FeO	47.08	46.69	44.61	41.28	47.66	40.42	46.69	47.21	48.02
MnO	1.15	1.12	1.23	0.96	1.07	0.80	1.15	0.84	1.17
MgO	1.06	1.48	1.59	3.67	1.32	8.60	5.02	4.99	4.43
Total	100.97	100.15	100.86	99.79	100.56	98.57	99.74	100.70	98.12
Si	0.014	0.000	0.000	0.000	0.000	0.043	0.010	0.010	0.062
Ti	4.425	4.578	3.981	3.948	4.699	5.149	5.549	5.495	5.892
Al	0.098	0.014	0.360	0.493	0.000	1.321	1.060	0.941	0.451
Cr	0.042	0.052	0.070	0.126	0.040	0.038	0.035	0.03	0.010
Fe^{3+}	6.963	6.765	7.295	7.484	6.549	4.303	3.782	4.045	3.381
Fe^{2+}	11.648	11.625	10.962	10.106	11.839	9.513	11.128	11.178	12.015
Mn	0.288	0.279	0.302	0.239	0.270	0.191	0.277	0.202	0.287
Mg	0.466	0.649	0.691	1.602	0.583	3.621	2.131	2.106	1.907

 * : FeO/Fe_2O_3 calculated assuming stoichiometric 3 cations per 4 oxygen

1,3,4 : Cores of phenocryst in xenolith

 2 : Microphenocryst in xenolith

 5 : Groundmass crystal occurring in the interstitial matrix of the xenolith

 6 : Phenocryst in the host lava

 7 : Core of phenocryst

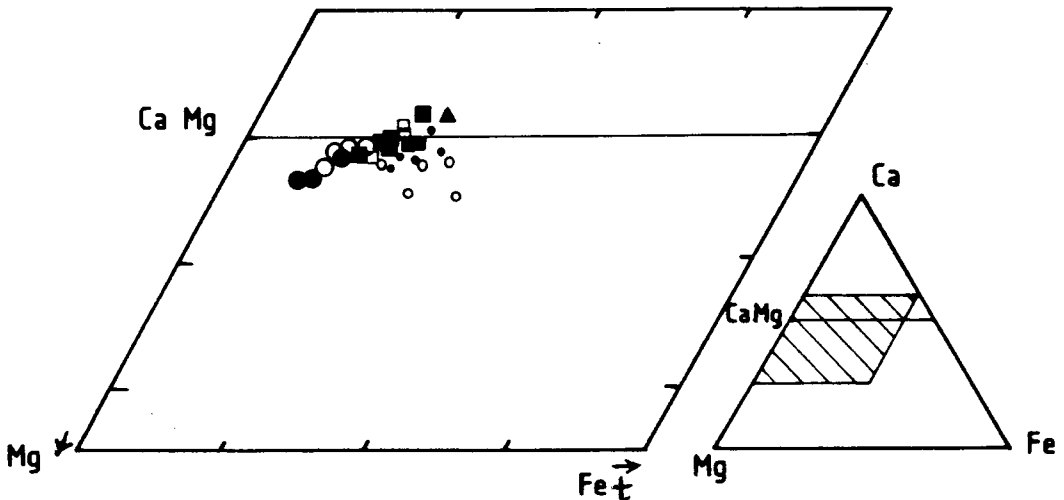 8 : Core of phenocryst

 9 : Groundmass crystal

FIG. 3. Clinopyroxene compositions plotted in the conventional Ca-Mg-Fe+Mn diagram, symbols as in Fig. 2.
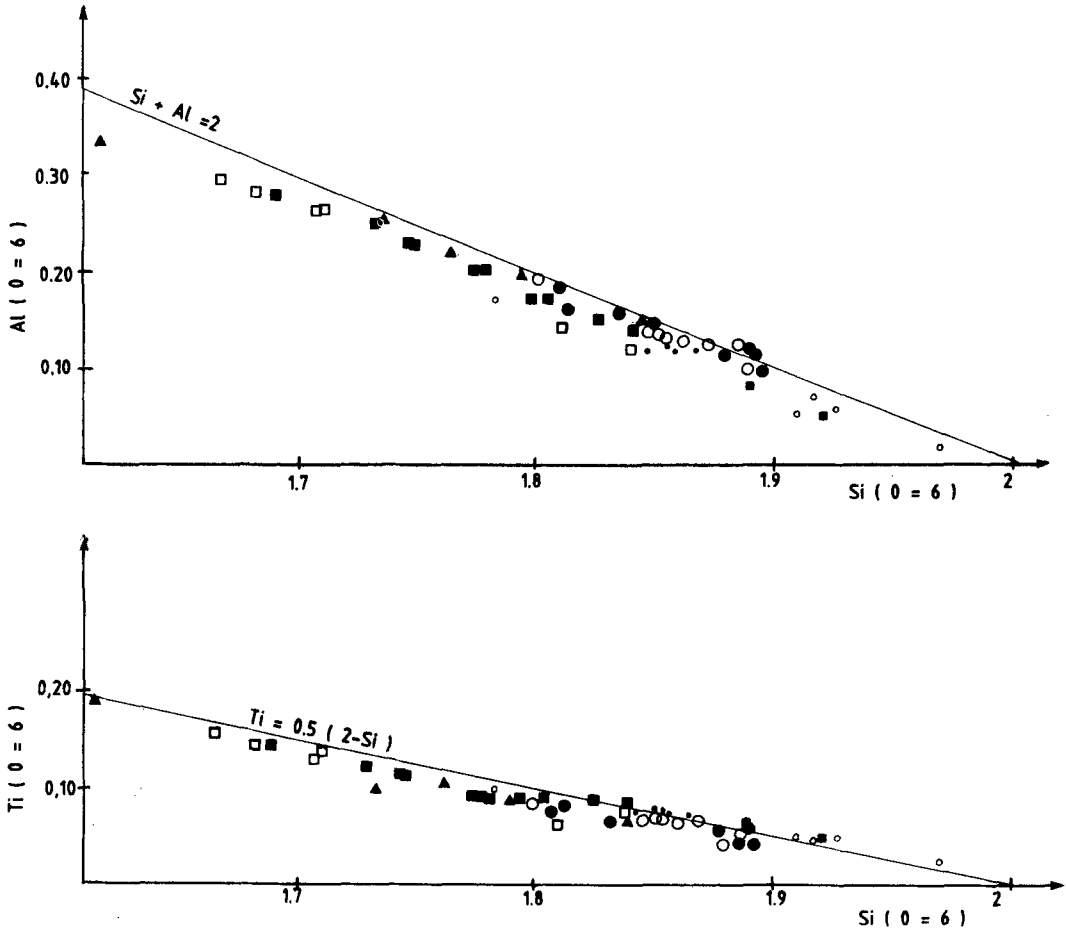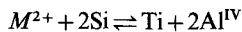
FIG. 4. Variations in aluminium and titanium with silica contents of the pyroxenes, symbols as in Fig. 2.

chemical continuity exists between megacryst cores, megacryst rims, phenocrysts and microphenocrysts and between the two samples. The sympathetic negative relationships between Al, Ti and Si, suggest that the dominant substitution is

$$M^{2+} + 2Si \rightleftharpoons Ti + 2Al^{IV}$$

There is a limited amount of $M^{2+} + Si \rightleftharpoons Al^{IV} + Al^{VI}$ type substitution which is only observed in Mg-rich (and Si-rich) pyroxenes, the molecule $M^+CrAlSiO_6$ being subordinate. To balance cation deficiency in the tetrahedral sites (Al $< 2 - Si$), Fe^{3+} is probably present in fourfold coordination in Si-poorer pyroxene compositions. Unlike Al and Ti, the Na contents of the pyroxenes do not appear to be strongly related to Si contents. So, it seems likely that the Na is present in the acmite molecule. This suggests that some of the main substitutions ('other' than quadrilateral components as defined by Papike et al., 1974) result from the charge-balance equation:

$$y^{Fe} + y^{Al} + y^{2Ti} + y^{Cr} \rightleftharpoons z^{Al} + z^{Fe} + x^{Na}$$
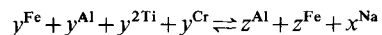
The megacryst compositional range is mainly controlled by the Ca–Mg substitution in site $M2$. Consequently, the incorporation of the $CaTiAl_2O_6$ component plays an essential role in the chemical trend of the clinopyroxenes. In the salite field, the Si and Al deficiencies imply in addition the introduction of ferri-Tschermak's molecules ($CaFe^{3+}Fe^{3+}SiO_6$; $CaTiFe^{3+}AlO_6$).

Starting from values of Mg/(Mg + Fe) < 0.75, the proportions of Ti and Al decrease while at site $M1$, the Ca–Fe substitution dominates. Such variations may be related to the fractionation of the Fe–Ti oxides (Gibb, 1973; Marcelot et al., 1985). Late-stage pyroxenes (including those in the groundmass) are characterized by a slight

TABLE 5 Pyroxene compositions

Sample	RW 100														RW 37							
N° of anal.	1	2	3	4	5	6	7	8	9	10	11	12	13'	14	13	14	15	16	17	18	19	20
SiO_2	50.72	48.44	50.78	46.54	42.18	47.38	50.23	50.47	49.84	48.12	49.61	46.54	50.96	50.32	48.10	45.78	49.14	46.21	45.43	50.63	50.34	49.11
TiO_2	1.52	2.44	1.44	3.67	6.64	3.57	1.44	1.90	2.35	3.03	2.20	3.67	1.56	1.88	3.20	4.46	3.25	4.16	4.53	1.70	2.36	2.79
Al_2O_3	2.72	3.53	2.24	4.93	7.38	3.88	2.86	2.05	2.86	4.42	2.80	4.93	1.63	1.14	3.94	5.75	3.43	5.10	5.97	1.19	1.93	2.70
Cr_2O_3	0.24	0.08	0.12	0.04	0.00	0.09	0.17	0.10	0.05	0.07	0.00	0.00	0.00	0.00	0.00	0.00	0.00	0.02	0.00	0.00	0.00	0.00
FeO	3.74	5.20	4.05	6.07	7.56	6.62	4.00	4.90	4.85	6.10	4.83	6.07	7.71	10.08	5.60	6.67	5.43	5.96	6.19	7.39	7.13	5.87
MnO	0.01	0.00	0.12	0.21	0.13	0.09	0.12	0.05	0.08	0.02	0.24	0.21	0.19	0.24	0.06	0.10	0.00	0.14	0.09	0.30	0.21	0.07
MgO	16.44	14.64	16.56	13.53	11.72	14.57	16.08	15.34	14.77	14.35	14.69	13.53	13.47	12.84	14.49	12.45	14.92	13.82	13.43	13.27	13.50	14.86
CaO	22.56	23.39	22.89	23.47	22.93	23.12	22.84	23.80	23.43	23.10	24.23	23.47	22.54	21.21	24.19	23.78	23.50	23.41	23.87	23.85	23.57	23.57
Na_2O	0.45	0.30	0.34	0.48	0.61	0.29	0.42	0.48	0.37	0.44	0.39	0.48	1.27	2.12	0.37	0.58	0.30	0.40	0.62	0.43	0.54	0.57
Total	98.42	98.02	98.54	98.94	99.15	99.61	96.16	99.09	98.60	99.65	96.99	98.90	99.33	99.83	99.95	99.57	99.97	99.22	100.13	98.76	99.58	99.54
Si	1.889	1.834	1.894	1.763	1.617	1.782	1.881	1.887	1.870	1.800	1.861	1.763	1.917	1.908	1.797	1.731	1.826	1.745	1.707	1.920	1.890	1.839
Ti	0.043	0.069	0.040	0.104	0.191	0.101	0.041	0.053	0.066	0.085	0.062	0.104	0.044	0.054	0.090	0.127	0.091	0.118	0.128	0.049	0.067	0.079
Al	0.119	0.158	0.098	0.220	0.333	0.172	0.126	0.090	0.126	0.195	0.124	0.220	0.072	0.051	0.173	0.256	0.150	0.227	0.265	0.053	0.085	0.119
Cr	0.007	0.003	0.004	0.001	0.000	0.003	0.005	0.003	0.003	0.002	0.000	0.000	0.000	0.000	0.000	0.000	0.000	0.001	0.000	0.000	0.000	0.000
Fe	0.116	0.165	0.126	0.192	0.242	0.208	0.125	0.153	0.152	0.191	0.151	0.192	0.243	0.320	0.175	0.211	0.169	0.188	0.194	0.234	0.224	0.184
Mn	0.001	0.000	0.004	0.007	0.004	0.003	0.004	0.002	0.001	0.005	0.008	0.007	0.006	0.008	0.002	0.003	0.000	0.004	0.003	0.009	0.006	0.002
Mg	0.912	0.826	0.921	0.764	0.670	0.817	0.898	0.855	0.826	0.800	0.821	0.764	0.755	0.726	0.807	0.702	0.826	0.778	0.752	0.750	0.755	0.830
Ca	0.901	0.949	0.915	0.952	0.942	0.932	0.917	0.953	0.942	0.926	0.974	0.952	0.908	0.862	0.968	0.963	0.935	0.947	0.961	0.969	0.948	0.946
Na	0.032	0.022	0.024	0.035	0.045	0.021	0.030	0.035	0.027	0.032	0.028	0.035	0.092	0.156	0.027	0.042	0.022	0.029	0.045	0.032	0.040	0.042
En	47.3	42.6	46.8	39.9	36.0	41.7	46.2	43.5	43.0	41.7	42.0	39.9	39.5	37.9	41.3	37.3	42.8	40.6	39.4	38.2	39.1	42.3
Fs	6.0	8.5	6.7	10.4	13.3	10.8	6.6	8.0	8.0	10.0	8.2	10.4	13.0	17.1	9.1	11.4	8.7	10.0	10.3	12.4	11.9	9.4
Wo	46.7	48.9	46.5	49.7	50.7	47.5	47.2	48.5	49.0	48.3	49.8	49.7	47.5	45.0	49.6	51.3	48.5	49.4	50.3	49.3	49.0	48.3

1 : Core of Cr-diopside megacryst occurring in the host lava
2 : Rim of the same megacryst
3 : Core of Cr-diopside megacryst (host lava)
4 : Core of microphenocryst (host lava)
5 : Groundmass crystal (host lava)
6 : Groundmass crystal (host lava)
7 : Core of megacryst (xenolith)

8 : Core of megacryst (xenolith)
9, 10 : Core and rim of the same phenocryst (xenolith)
11, 12 : Core and rim of the same phenocryst (xenolith)
13, 14 : Groundmass crystals (xenolith)

13, 14 : Core and rim of phenocryst
15, 16 : Cores of phenocryst
17 : Core of microphenocryst
18, 19 : Groundmass crystals
20 : Small microphenocryst

TABLE 6   Phlogopite compositions

Sample	RW 100							
N° of anal.	1	2	3	4	5	6	7	8
SiO₂	38.13	38.74	40.53	35.86	35.12	35.46	35.47	38.91
TiO₂	6.07	6.00	5.90	7.97	8.04	8.05	7.63	7.75
Al₂O₃	11.31	10.67	10.39	15.23	14.83	14.86	13.74	12.32
Cr₂O₃	0.10	0.00	0.44	0.07	0.00	0.00	0.00	0.00
FeO	7.74	7.66	5.85	9.15	8.10	8.28	9.08	7.16
MnO	0.17	0.16	0.17	0.00	0.08	0.04	0.01	0.07
MgO	20.47	20.28	21.60	17.42	18.07	17.85	17.79	18.36
CaO	0.02	0.00	0.00	0.02	0.00	0.00	0.00	0.00
Na₂O	0.53	0.63	0.50	0.18	0.17	0.17	0.24	0.49
K₂O	9.81	9.89	10.43	10.10	10.57	10.52	10.36	10.26
Total	94.35	94.03	95.81	96.00	94.98	95.23	94.32	95.32
Si	5.729	5.835	5.837	5.210	5.177	5.210	5.283	5.660
Ti	0.760	0.753	0.639	0.871	0.891	0.889	0.855	0.850
Al	2.003	1.894	1.763	2.609	2.577	2.572	2.413	2.109
Cr	0.012	0.000	0.050	0.008	0.000	0.000	0.000	0.000
Fe	0.972	0.965	0.704	1.112	0.998	1.017	1.132	0.869
Mn	0.021	0.021	0.020	0.000	0.010	0.004	0.001	0.009
Mg	4.584	4.553	4.637	3.771	3.970	3.909	3.951	3.984
Ca	0.003	0.000	0.000	0.003	0.000	0.000	0.000	0.000
Na	0.155	0.183	0.139	0.050	0.048	0.048	0.068	0.136
K	1.879	1.901	1.917	1.872	1.987	1.972	1.968	1.950
$\frac{Mg \times 100}{Mg + Fe_t}$	82.2	82.2	86.5	77.2	79.8	79.3	77.7	82.1

1,2 : Core of megacryst occurring outside the xenolith
  3 : Core of a strongly resorbed megacryst in the xenolith
  4 : Rim of the same megacryst
  5 : Rim of a strongly resorbed megacryst in the xenolith
6,7,8 : Core of microphenocryst

increase in iron and sodium. Enrichment of Na in later crystallized salites, probably as acmite and minor $NaTiFe^{3+}SiO_6$, reflects the alkali enrichment of residual liquids. However, groundmass pyroxenes occurring in the xenolith show a distinct trend of acmite enrichment.

The phlogopite megacrysts occurring in the coarse-grained xenolith are essentially identical in composition to those scattered in the lava. As in the case with the pyroxene, their chemical composition varies significantly from core to rim. Outer rims are quite similar to microphenocrysts and correspond to the most evolved compositions.

The phlogopites are titaniferous with typically low alumina contents. The amounts of Ti, K, Al increase with decreasing $Mg/(Mg+Fe)$ whereas the Si contents decrease. In fact the atomic proportions of Al (< 2.7 at. for 22 oxygens) and Si (< 6 at. for 22 oxygens) are so low that the tetrahedral sites cannot be filled, suggesting the presence of Fe^{3+} in the Z-component. The cation

deficiency slightly decreases towards more Fe-rich compositions which corresponds to a clear increase of the Al/Si ratios.

Compositional variation of phlogopites are plotted in Fig. 5 in terms of $2Al^{IV} + Ti$ versus $2Si + Mg$. As shown by the regular negative correlations, the progressive incorporation of Ti^{4+} into the phlogopite structure must be achieved by the dominant coupled substitution (Robert, 1976; Wendlandt, 1977):

$$2Al^{IV} + Ti^{VI} \rightleftharpoons 2Si^{IV} + Mg^{IV}$$
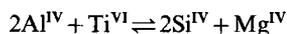
This substitution becomes more important towards more evolved crystals, which is consistent with lower-pressure regimes of crystallization (Edgar *et al.*, 1976; Robert, 1976). The interlayer site is usually complete, in spite of the increase in K/Na ratio with decreasing $Mg/(Mg+Fe)$, the sum of K + Na remaining almost constant.

Interstitial glass. Microprobe analyses show enrichment in Al, Na, K and depletion in Mg, Ti
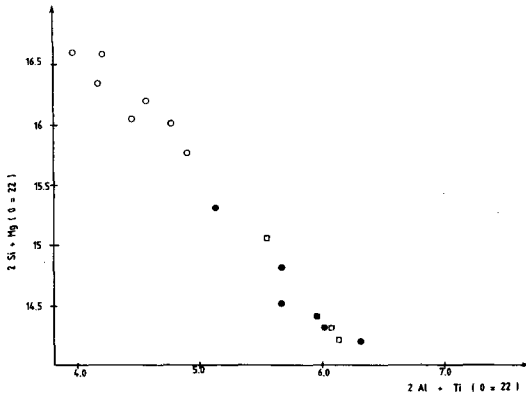
FIG. 5. Diagram illustrating the role of $2Al^{IV} + Ti = 2Si + Mg$ substitution in phenocryst core (open circle), phenocrysts rim (open square) and microphenocrysts (filled circle) phlogopite.

TABLE 7   Electron microprobe analysis of glasses of host rock.

N° of anal.	1	2
SiO₂	40.97	40.17
TiO₂	4.57	4.47
Al₂O₃	14.55	14.19
FeO_t	6.56	8.59
MnO	0.10	0.15
MgO	5.73	5.66
CaO	13.06	12.26
Na₂O	6.84	7.17
K₂O	6.05	5.39
Total	98.43	98.05

1 : Interstitial glass in groundmass

2 : Interstitial glass near xenolith

and Fe, relative to the whole rock. The glass probably formed in the same lava and has a somewhat similar composition, with only minor out-range concentrations for Na_2O and FeO. In addition to the relative homogeneity of the glass, we note the lack of strong concentration gradients near the xenolith surface.

Discussion

Petrographical and mineralogical data provide evidence that the megacrysts were not in equilibrium with the host magma during eruption. The resorption observed in some crystals probably occurred during a pressure drop, revealing earlier crystallization at depth. The pyroxenes and phlogopites occurring as megacrysts in the host lava are very similar in composition to those in the xenolith. It is, therefore, likely that these megacrysts were derived from the disaggregation of the xenolith. The observed trend of increasing $Ca/(Ca + Fe + Mg)$, together Ti, Al and Fe^{3+} in pyroxenes is believed to reflect progressive crystallization and attendant physical changes of an undersaturated mafic parent magma (Irving, 1974). Likewise, the increased Ti substitution in phlogopite (from core to rim or to microphenocryst) is considered to be due mainly to a rather large pressure drop of the fractionating magma.

The typical reaction rim surrounding olivine phenocrysts, common in some potassic rocks (Holmes and Harwood, 1937; Carmichael, 1967), is strong evidence that the crystallization of mica and pyroxene occurs according to the reaction

proposed by Modreski and Boettcher (1973) and Barton and Hamilton (1978):

$$olivine + L \rightleftharpoons phlogopite + CPX + vapour$$

Phase equilibria, presented by Luth (1967), show that ultrapotassic magma at depth, initially precipitating olivine, should cool with resorption of olivine and formation of mica and pyroxene. The presence of leucite, along with these two later phases, suggests that the rocks were produced by a long cooling differentiation process at moderate pressure, followed by a final equibration at shallow depths. During the ascent of the magma, the concentration of the vapour phase in the liquid tends to decrease and the field of phlogopite would be reduced. Assuming such a model of evolution, the differentiated liquid would be in the leucite field, this being enlarged with decreasing volatile component (Luth, 1967). The lack of phlogopite in the groundmass indicates that the contents of $H_2O + F$ was not great enough for the phlogopite volume to equal the leucite volume (Brown and Carmichael, 1969).

Comparison of the main chemical parameters of the phlogopites with those from various localities (e.g. Edgar and Arima, 1983), indicates that these phlogopites represent early products from a crystallizing liquid. The distinctly high K/Al (> 1) and K/Ti (> 3) ratios cause a cation deficiency and a slight tendency to Si–Al substitution in the Z-site. A similar phenomenon (Al-poor character) is found in the pyroxenes and Fe–Ti oxides. Despite the Si-poor nature of host rocks, the amount of Tschermak's molecule is relatively low, reflecting the moderate replacement of Al for Si in fourfold coordination. This suggests that the peralkaline character (or paucity in alumina) of the primary liquid played a greater role than the

level of silica undersaturation. Thus, the compositions of early-formed phlogopite and pyroxene are considered to be sufficiently silica-rich to inhibit any increasing level of silica activity in the residual melt. Compositional variations of ferromagnesian megacrysts and phenocrysts (increasing in Al and Ti contents), successive parageneses and compositions of interstitial glasses confirm that the fractionation trends lead to a silica-poor residual. Removal of the crystalline phases tends to lower the degree of undersaturation, this view is supported by comparisons with the evolution of the leucitites from the Leucite Hills province (Carmichael, 1967), Roman province (Cundari, 1975) or Gaussberg province (Sheraton and Cundari, 1980). According to chemical characteristics of early-formed crystals, the liquid followed a fractional crystallization trend towards a Si-poor or Si-rich residual.

It, therefore, appears likely that a magma with $K + Na > Al$ may represent the melt from which the early paragenesis formed. Accordingly, the peralkaline nature of the host rock is believed to reflect a primary geochemical characteristic of the initial melt (Barton and Hamilton, 1982).

Acknowledgements

References

Barton, M. and Hamilton, D. L. (1978) *Contrib. Mineral. Petrol.* **66**, 41–9.
——————(1982) *Mineral. Mag.* **45**, 267–78.
Bell, K. and Powell, J. L. (1969) *J. Petrol.* **10**, 536–72.
Brown, F. H. and Carmichael, I. S. E. (1969) *Lithos*, **2**, 239–60.
Carmichael, I. S. E. (1967) *Contrib. Mineral. Petrol.* **15**, 24–66.
Cundari, A. (1975) Ibid. **53**, 129–44.

Denaeyer, M.-E. (1972) *Ann. Mus. Roy. Afr. Centr., Tervuren, Geol. Ser.* no. 72.
——and Schellinck (1965) Ibid. no. 49.
Edgar, A. D. and Arima, M. (1983) *Mineral. Mag.* **47**, 11–19.
——Green, D. H., and Hibberson, W. O. (1976) *J. Petrol.* **17**, 339–56.
Faust, G. T. (1963) *Schweiz. Mineral. Petrogr. Mitt.* **43**, 165–95.
Frey, F. A., Green, D. H., and Roy, S. D. (1978) *J. Petrol.* **19**, 465–513.
Gibb, J. G. A. (1973) Ibid. **14**, 203–30.
Guibert, P. (1978) Thesis Univ. Geneve, 152 pp.
Gupta, A. K. and Yagi, D. (1980) In *Petrology and genesis of leucite-bearing rocks.* (P. J. Wyllie, ed.), Chicago.
Holmes, A. and Harwood, H. F. (1937) *Mem. Geol. Surv. Uganda*, **3**, 1–300.
Irving, A. J. (1974) *Bull. Geol. Soc. Am.* **85**, 1503–14.
Luth, W. C. (1967) *J. Petrol.* **8**, 372–416.
Marcelot, G., Rançon, J. P., and Demange, J. (1985) *J. Volcanol. Geotherm. Res.* **26**, 99–129.
Modreski, P. J. and Boettcher, A. L. (1973) *Am. J. Sci.* **273**, 385–414.
Papike, J. J., Cameron, K. L., and Baldwin, K. (1974) *Geol. Soc. Am. Abstracts With Programs*, **6**, 1053–54.
Pouclet, A. (1976) Thesis. Univ. Paris Sud 610 pp.
——————(1977) *Rev. Geogr. Phys. Geol. Dyn.* **2**, 19 (2), 115–24.
——Menot, R. P., and Piboule, M. (1983) *Bull. Mineral.*, **106**, 607–22.
Rançon, J. P. and Demange, J. (1983) *Rapport BRGM*, 192 GTH, 130 pp.
Robert, J. L. (1976) *Chem. Geol.* **17**, 213–27.
Sheraton, J. W. and Cundari, A. (1980) *Contrib. Mineral. Petrol.* **71**, 417–27.
Shervais, J. W. (1982) *Earth Planet. Sci. Lett.* **59**, 101–18.
Simkin, T. and Smith, J. V. (1970) *J. Geol.* **78**, 207–19.
Stormer, J. C. (1973) *Geochim. Cosmochim. Acta.* **37**, 1815–21.
Thonnard, R. L. G., Denaeyer, M. E., and Antun, P. (1965) *Carte volcanologique des Virunga au 1/50 000e*. Institut Géographique Militaire—Bruxelles.
Van Kooten, G. K. (1980) *J. Petrol.* **21**, 651–84.
Wendlandt, R. F. (1977) *Carnegie Inst. Washington Yearb.* **77**, 534–9.